Article

Recent reduced abyssal overturning and ventilation in the Australian Antarctic Basin

Kathryn L. Gunn [1,2] ✉, Stephen R. Rintoul [1,3], Matthew H. England [4] & Melissa M. Bowen [5]

Dense water formed near Antarctica, known as Antarctic bottom water (AABW), drives deep ocean circulation and supplies oxygen to the abyssal ocean. Observations show that AABW has freshened and contracted since the 1960s, yet the drivers of these changes and their impact remain uncertain. Here, using observations from the Australian Antarctic Basin, we show that AABW transport reduced by 4.0 Sv between 1994 and 2009, during a period of strong freshening on the continental shelf. An increase in shelf water salinity between 2009 and 2018, previously linked to transient climate variability, drove a partial recovery (2.2 Sv) of AABW transport. Over the full period (1994 to 2017), the net slowdown of -0.8 ± 0.5 Sv decade^{-1} thinned well-oxygenated layers, driving deoxygenation of -3 ± 2 µmol kg^{-1} decade^{-1}. These findings demonstrate that freshening of Antarctic shelf waters weakens the lower limb of the abyssal overturning circulation and reduces deep ocean oxygen content.

Antarctic bottom water (AABW) is formed when dense water sinks from the Antarctic shelf to the abyssal ocean, entraining fluid as it descends. Newly formed oxygen-rich AABW spreads north and fills up to 40% of the total volume of the global ocean, driving the lower limb of the global overturning circulation and renewing oxygen in (ventilating) the abyssal ocean interior[1,2]. Past studies have highlighted rapid and widespread changes in the volume and salinity of AABW, with implications for global ocean circulation[3–10]. However, observations of the abyssal Southern Ocean are sparse in space and time. Consequently, the drivers and impacts of variability in AABW properties and circulation remain poorly understood.

The precursor of AABW is cold, relatively salty and oxygen-rich dense shelf water (DSW) formed on the Antarctic continental shelf by wintertime cooling and brine rejection. Shelf water of sufficient density to produce AABW is formed in four distinct regions of the Antarctic margin: namely, the Weddell Sea, Cape Darnley, the Adélie Land Coast and the Ross Sea. DSW exported from these shelf regions mixes with lighter water as it descends the continental slope to form AABW. While contraction and freshening have been observed in each of the AABW varieties, some of the largest changes have occurred in Ross Sea bottom water (RSBW)[3–5,7] which supplies the abyssal layer of the Pacific and eastern Indian basins[11]. The multidecadal freshening of RSBW has been linked to freshening of DSW on the Ross Sea shelf[12,13], which in turn has been attributed to increased supply of glacial meltwater from the Amundsen Sea[13,14].

AABW is the primary source of oxygen to the abyssal ocean, therefore changes in AABW production will impact oxygen concentrations in the deep ocean[15,16]. Observations of oxygen inventory show large decreases in the abyssal Southern Ocean, suggesting a decline in bottom water ventilation (deoxygenation)[17]. Models have also linked reduced deep overturning to ongoing reductions in abyssal ocean ventilation and oxygen in a changing climate[15,18]. Yet, the maximum oxygen concentration observed in the AABW layer has not changed significantly with time[7,19], suggesting that oxygen-rich bottom water has continued to sink to the abyss around Antarctica but at somewhat lighter densities[5,7,8].

Contraction and freshening of AABW may reflect changes in either its formation rate or source water properties[2,3,5,7]. Decreases

[1]CSIRO Environment, Hobart, Tasmania, Australia. [2]School of Ocean and Earth Science, University of Southampton, Southampton, UK. [3]Australian Antarctic Program Partnership, University of Tasmania, Hobart, Tasmania, Australia. [4]Climate Change Research Centre (CCRC) and Australian Centre for Excellence in Antarctic Science (ACEAS), University of New South Wales, Sydney, New South Wales, Australia. [5]School of Environment and Climate Systems Laboratory, University of Auckland, Auckland, New Zealand. ✉e-mail: k.gunn@soton.ac.uk
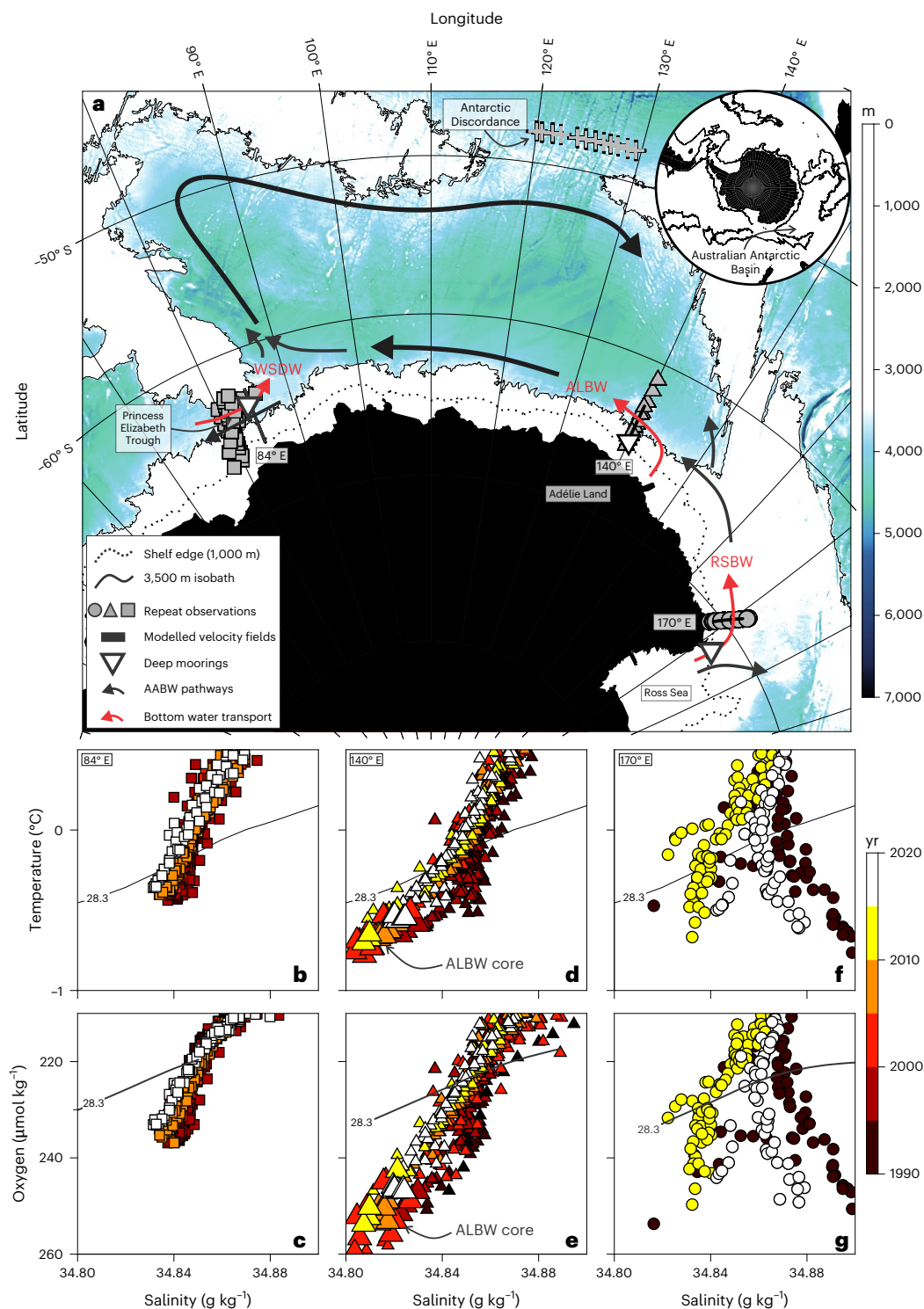
Fig. 1 | Abyssal circulation and characteristics of water masses in the Australian Antarctic Basin. a, Bathymetric map where thin dotted and solid black lines trace shelf edge (1,000 m) and basin-mean shallowest depth of AABW (3,500; defined here as $\gamma \geq 28.30$ kg m^{-3}); red arrows and labels show where WSDW, ALBW and RSBW enter basin; black arrows, resultant flow of AABW; white triangles, deep moorings (Table 1); grey crosses, bottle casts collected at 48° S (Supplementary Fig. 1); grey square/triangle/circle symbols, loci of bottle casts collected during repeat hydrographic surveys at 84° E/140° E/170° E (Supplementary Table 1); thick black lines, cross-sections extracted from model. The inset highlights the global location of Australian Antarctic Basin shown in **a**. **b**, Conservative temperature–absolute salinity diagram of bottle measurements collected near 84° E coloured for year of acquisition; thin black line, neutral density contour of 28.30 kg m^{-3}. **c**, Dissolved oxygen concentration–absolute salinity of bottle measurements collected at 84° E (note that the oxygen scale is inverted). Symbols as in **b**. **d,e**, Same as **b** and **c** for bottle measurements collected at 140° E. Enlarged symbols, measurements from ALBW core (Methods). **f,g**, Same as **b** and **c** for bottle measurements collected at 170° E.

in AABW volume have been interpreted as evidence of a reduction in bottom water formation and slowing of the overturning circulation[3,10] but direct measurements of changes in AABW transport are not available to test this hypothesis. The loss of the densest classes of AABW could also be explained by freshening of DSW and a shift to formation of lighter density classes of AABW[7]. It is therefore not yet

Table 1 | Mooring data used in this study

Name	Date	Location	Pressure	Density	Speed	Shear
		°E, °N	dbar	kg m^{-3}	m s^{-1}	×10^{-4} s^{-1}
ADOX	February 1993–March 1994	84.0, −63.5	3,002	28.36 (0.01)	0.00 (0.03)	−0.7 (0.8)
ALCS	January 1995–January 1996	140.0, −65.2	2,632	28.35 (0.02)	0.15 (0.04)	1.2 (0.4)
CALM	January 2008–January 2011	172.3, −71.5	1,840	28.34 (0.04)	0.16 (0.09)	2.3 (2.0)

Time mean of bottom pressure, neutral density and cross-sectional speed (values recorded at deepest mooring). Vertical velocity shear calculated using moorings 270, 854 and 440 dbar above deepest mooring of each experiment on average. Positive speed and shear values indicate flow into Australian Antarctic Basin and speed increase with depth, respectively. Values inside brackets denote standard deviations. ADOX, Antarctic deep outflow experiment[28,43] (density calculated from time series of in situ temperature and practical salinity of 34.75 psu); ALCS, Adélie Land continental slope experiment[44] (data digitized from ref. 44 and representing absolute speed, rather than cross-sectional velocity and density calculated from time series of in situ temperature and practical salinity of 34.67 psu); CALM, Cape Adare long-term monitoring experiment[45,46].

clear whether the multidecadal changes in AABW reflect changes in the amount of AABW formed, changes in the properties of DSW or a combination of the two.

Motivated by these results, we investigate the drivers of AABW change and its impact on abyssal circulation and ventilation using an observation-driven approach to quantify variability in volume and oxygen transport. We focus on the Australian Antarctic Basin as it is the best-ventilated Antarctic basin[1] and therefore likely to provide the earliest signal of change in abyssal ocean ventilation. The basin also lies downstream of the large and increasing sources of glacial meltwater input in the Amundsen Sea[13,20,21]. We quantify changes in the properties and amount of bottom water entering the basin by combining repeat hydrographic observations, direct velocity measurements and flow structure derived from a 0.1° global ocean sea-ice model that realistically simulates AABW formation sites and export pathways[11,22,23]. The transport estimates show that the lower limb of the overturning circulation in the Australian Antarctic Basin has slowed overall during the past three decades, driving deoxygenation of the deep ocean.

Bottom water freshening and contraction

The Australian Antarctic Basin is supplied by three different sources of AABW (defined as water with neutral density $\gamma \geq 28.30$ kg m^{-3} following refs. 7,19). These bottom waters enter the basin through topographic gateways at 84° E (Weddell Sea deep water, WSDW), 140° E (Adélie Land bottom water, ALBW) and 170° E (RSBW) (Fig. 1a). Multidecadal variability in AABW properties is clear in the conservative temperature–absolute salinity (hereafter temperature and salinity) and salinity–dissolved oxygen concentration (hereafter oxygen) relationship at each section (Fig. 1b–g). We use observations from these three gateways to quantify changes in the properties and transport of AABW (Methods and Supplementary Section 1).

Bottom waters entering the Australian Antarctic Basin have generally become fresher, lighter and contracted in volume since the 1990s (Figs. 1 and 2 and Extended Data Figs. 1–3). RSBW shows the greatest changes: between the 1992 and 2011 occupations of the 170° E section, the mean salinity of the layer with neutral density ≥28.30 kg m^{-3} decreased by 0.04 g kg^{-1} and the area of the layer decreased by 70% (Figs. 1f,g and 2g–i). Between the 2011 and 2018 occupations, the salinity of the RSBW layer rebounded by 0.03 g kg^{-1} and its area returned to values similar to those observed in 1992. The salinity and area of ALBW and WSDW also decreased between the early 1990s and late 2010s but the changes are smaller than observed in RSBW (Figs. 1b–e and 2a–f). While the AABW salinity, density and volume decreased, the dissolved oxygen concentration in the layer denser than ≥28.30 kg m^{-3} remained high, with a slight increase of 1–3 μmol kg^{-1} at each location between 1992 and 2018 that is close to the threshold of uncertainty (Fig. 2 and Extended Data Fig. 4). Thus, the freshening and contraction of bottom water documented in earlier studies (based on data collected before 2013; for example, refs. 5,7,8) has continued into the late 2010s. Dissolved oxygen concentrations have remained stable, as seen in data before 2011 (ref. 7). Observations from the three gateways indicate

that RSBW has the greatest variability and therefore is the most likely driver of AABW changes in the Australian Antarctic Basin.

Bottom water flow variation

Measurements from single moorings at each gateway reveal that the speed of bottom water flow into the Australian Antarctic Basin varies with location, season and density (Fig. 3a,c,e). The mean speed of RSBW is 0.16 ± 0.09 m s^{-1}. ALBW has similar mean speed but smaller variability (0.15 ± 0.04 m s^{-1}). At 84° E, the mean speed of bottom water entering the basin through the Princess Elizabeth Trough is 0 ± 0.03 m s^{-1}. The vertical velocity shear, calculated across the few hundred metres between the deepest two current meters on each mooring, is of order 1×10^{-4} s^{-1} (positive values indicate speed increases with depth; Table 1). Depending on location, the temporal changes in bottom speed follow the seasonal effects of winds[24,25], tides[26,27], DSW formation and barotropic jet migration[28] that can delay and enhance flow at each gateway.

The near-bottom speed is correlated with near-bottom neutral density ($r^2 = 0.6$) for RSBW and ALBW, whereby greater densities result in faster flow (Fig. 3a,c,e). This correlation is expected in regions close to the DSW source locations where flows behave as density-driven plumes[29–32]. In contrast, flow speeds at 84° E do not exhibit a strong correlation with density, since this flow is remote from its source.

The mooring observations at each gateway do not span the AABW layer. To estimate the horizontal structure of the bottom water flow in the absence of adequate measurements, we use a high-resolution global ocean model that captures realistic DSW and AABW production[22,23]. The horizontal structure of the bottom water flows are determined using output from the model (Extended Data Fig. 5). These modelled structure functions—normalized, γ-mean cross-sectional speeds—reveal that the horizontal structure of bottom water flow varies at each location but changes little on seasonal timescales (Fig. 3b,d,f). For RSBW, the bottom water outflow forms a 50 km wide jet banked against the continental slope and its strength decays rapidly to the north. ALBW has two cores: a narrow 30 km wide jet banked against the slope and a slower and broader (70 km wide) jet that is centred at around −64.25° N. At 84° E, the horizontal structure shows eastward transport of WSDW in the north and westward transport of ALBW and RSBW in the south, as expected (Fig. 3b). At each gateway, the horizontal structure of the bottom water flow is stable in time (Fig. 3b,d,f). We combine point velocity measurements from the moorings, which provide detailed information about how AABW speed varies with density and season (Fig. 3a,c,e), with the structure functions (Fig. 3b,d,f) and observed changes in near-bottom neutral density (Extended Data Fig. 4), to determine bottom water volume transport (Methods). This new joint mooring-model-hydrographic approach exploits the strengths of each dataset and produces reliable estimates of changes in volume transport (Extended Data Fig. 6 and Supplementary Section 2).

Changes in transport and abyssal overturning

The calculated 1992 to 2018 time series of volume and oxygen transport are shown in Fig. 4a,b. The time mean volume transport of RSBW is
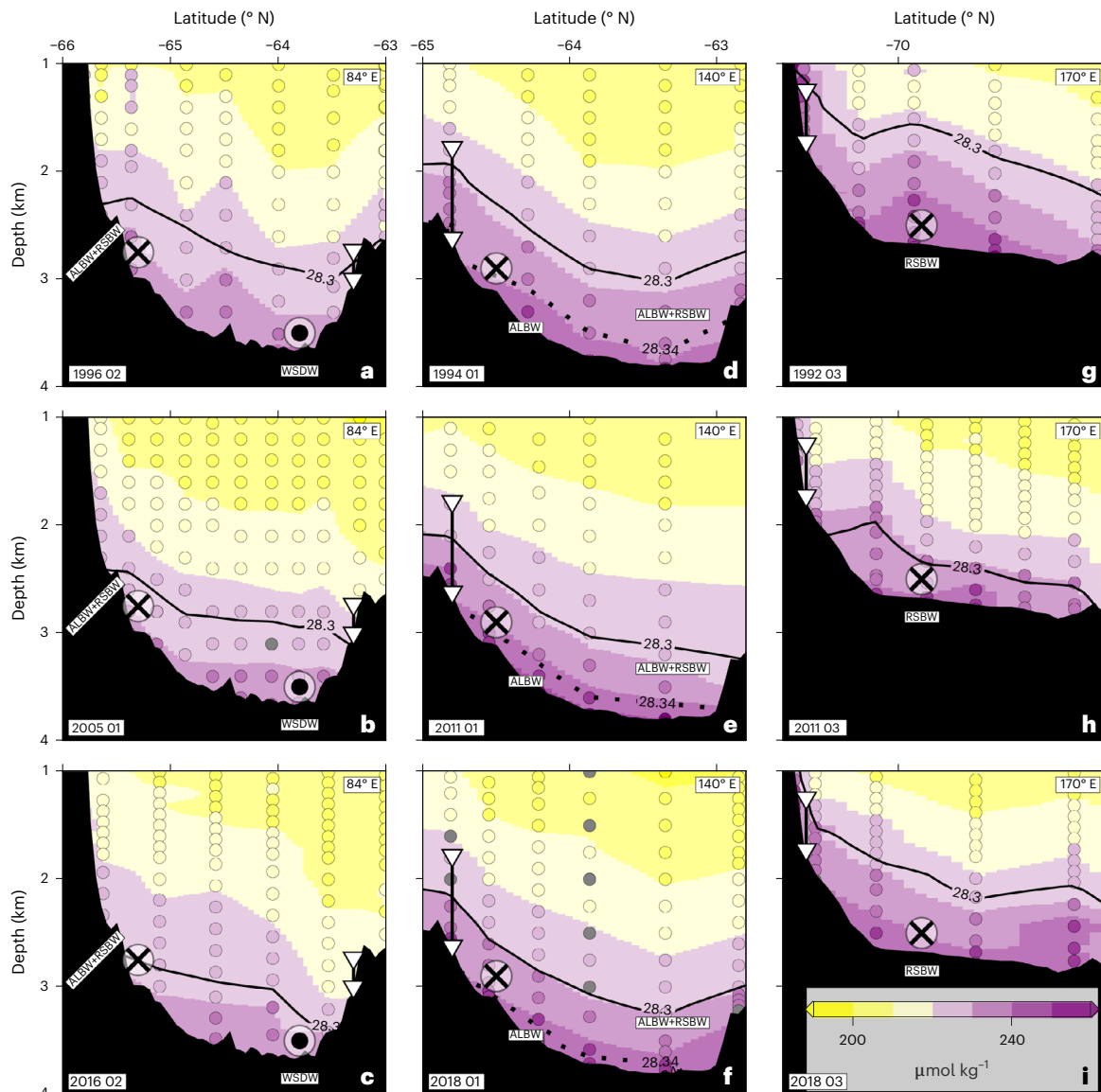
Fig. 2 | Latitude–depth sections of dissolved oxygen concentration over time and space using repeat hydrographic data. a, Mapped cross-section of oxygen for water masses along 84° E interpolated from data collected along I08S in February 1996. Coloured shading, interpolated oxygen of water masses coloured according to scale shown in **i**; outlined circles, bottle samples of oxygen shaded using the same scale; black polygon, bathymetry across section; thick black line, 28.30 kg m^{-3} neutral density threshold used to define AABW at 84° E and 170° E; thick dotted line, 28.34 kg m^{-3} neutral density threshold used to define AABW at 140° E; white triangles connected by line, loci of current meters projected onto

section using water depth at each mooring[28,43–46] (Table 1); bottom water varieties and flow direction shown schematically and annotated (circled cross/dot indicates flow into/out of page). **b**, Same as in **a** for data collected during January 2005. **c**, Same as in **a** for data collected during February 2016. **d**–**f**, Oxygen of water masses at 140° E interpolated from data collected along SR03 in January of 1994, 2011 and 2018. Symbols as before. **g**–**i**, Oxygen of water masses at 170° E interpolated from data collected along S04P in March of 1992, 2011 and 2018. Symbols as before. Note different latitude scales.

3.2 ± 0.6 Sv. Between 1992 and 2011, RSBW volume transport decreased by 65% from 4.3 to 1.5 Sv, then recovered to 3.7 Sv in 2018. The mean volume transport of the core of ALBW (see definition in Methods) is 0.7 ± 0.1 Sv; its transport decreased by 77% from 1994 to 2018. The net exchange of bottom water at 84° E is positive (that is, into the basin) for most summer seasons with a mean magnitude of 0.2 ± 1.0 Sv.

The sum of the time mean bottom water transports, 4.1 ± 1.2 Sv, is a measure of the average strength of the lower limb ($\gamma \geq 28.30$ kg m^{-3}) of the Southern Ocean overturning circulation in the Australian Antarctic Basin between the early 1990s and late 2010s. To assess variations in the strength of this overturning, we average the transport estimates for three time periods for which repeat hydrographic sections are available at each gateway (1992–1996, 2007–2011 and 2016–2018). Summing the

results gives the total transport of AABW into the basin for the periods centred on the years 1994 (5.9 Sv), 2009 (1.9 Sv) and 2017 (4.1 Sv). Between 1994 and 2009, the overturning slowed by −2.8 ± 0.5 Sv decade^{-1}. The overturning strengthened between 2009 and 2017, due to the recovery of RSBW formation in 2014–2016. Over the full period from 1994 to 2017, the overturning weakened by −0.8 ± 0.5 Sv decade^{-1}.

As well as slowing the lower limb of Southern Ocean overturning, the reduction in formation and export of AABW also caused the bottom water layer to thin. Between 1994 and 2009, the 28.30 kg m^{-3} isopycnal descended by 120 ± 35 m decade^{-1} (Methods), consistent with findings in earlier studies[3,7]. The post-2014 recovery of Ross shelf water salinity[12,33] and RSBW transport partially offset this thinning but, for the basin as a whole, AABW continued to thin into the late 2010s[34].
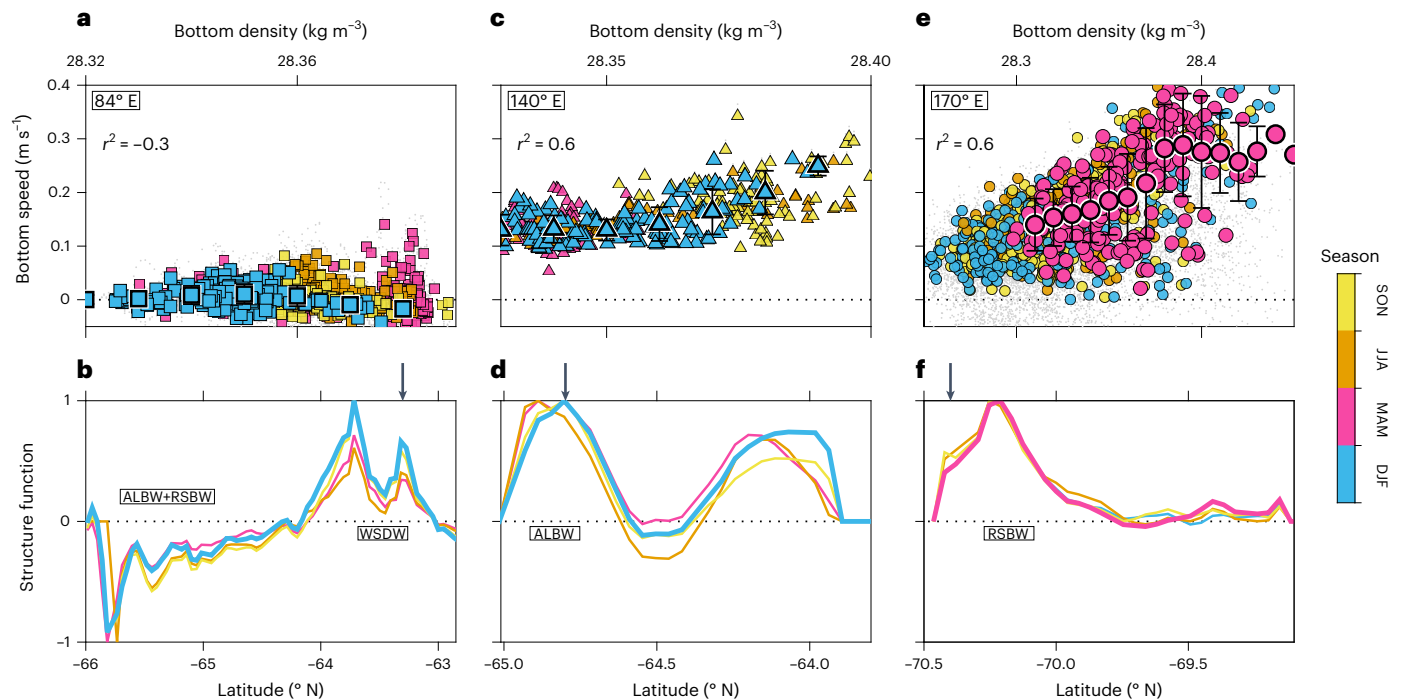
Fig. 3 | Bottom water strength and structure from mooring and model data. a, Near-bottom cross-sectional speed and neutral density from mooring at 84° E with correlation coefficients shown in top left. Grey circles, hourly measurements of bottom speed and neutral density; coloured shapes, daily means coloured by season according to scale; outlined shapes, seasonal mean speeds ± standard deviation as calculated in density bins of 0.01 kg m^{-3} (means only shown for season of repeat hydrographic data that are used as v_b in equation (1)); positive values indicate flow into Australian Antarctic Basin. **b**, Structure function calculated as normalized, γ-mean cross-sectional speed along AABW

layer from model. Coloured lines, seasonal means for 1990–2018 coloured according to scale; black arrow on top axis, location of mooring projected onto section using its water depth; positive values indicate flow into Australian Antarctic Basin with bottom waters annotated at latitude of entry/exit to basin. **c,d**, Same as in **a** and **b** for 140° E. **e,f**, Same as in **a** and **b** for 170° E. See Table 1 and Figs. 1a and 2 for mooring loci, deployment periods and statistics[28,43–46]. SON, September, October, November; JJA, June, July, August; MAM, March, April, May; DJF, December, January, February.

Over the full period from 1994 to 2017, the slowdown in overturning of −0.8 ± 0.5 Sv decade^{-1} caused a mean isopycnal descent rate of 60 ± 35 m decade^{-1}.

Reduced ventilation of the abyss

Oxygen transports, which provide direct estimates of ventilation, reveal that RSBW and ALBW contribute the most oxygen to the deep Australian Antarctic Basin (Fig. 4b). On average, RSBW and ALBW deliver 740 ± 180 and 150 ± 30 Sv mol kg^{-1} of oxygen to the basin, respectively, whilst WSDW contributes a negligible amount of 20 ± 220 Sv mol kg^{-1}. At each section, the variability in oxygen transport is dominated by changes in volume transport, rather than changes in dissolved oxygen concentration (Extended Data Fig. 4). The reduction in AABW transport between 1994 and 2017 resulted in a 28% decline in oxygen transport to the abyssal Australian Antarctic Basin (Fig. 4b).

Our results support the suggestion that slowdown of the overturning circulation results in deoxygenation of the deep ocean[15,16] and provide new insight into the mechanisms of reduced ventilation. First, slowing of the overturning reduces the transport of oxygen to the abyss. We estimate that the reduction in AABW transport between 1994 and 2009 resulted in a 3 ± 2 µmol kg^{-1} decade^{-1} decline in oxygen concentration below 3,500 m in the Australian Antarctic Basin (Methods). For the full period between 1994 and 2017, the decline is 1 ± 2 µmol kg^{-1} decade^{-1} and is not significant. Second, the contraction of AABW also drives deoxygenation; as the AABW layer thins, well-ventilated AABW is replaced by CDW that is lower in oxygen, resulting in a reduction in oxygen on pressure surfaces (Methods). The decrease in volume transport between 1994 and 2009 is associated with a 120 ± 35 m decade^{-1} descent of the isopycnal defining the top of the AABW layer, averaged

over the basin. This contraction of the well-ventilated layers results in an oxygen decline of 6 ± 2 µmol kg^{-1} decade^{-1}. For the full period between 1994 and 2017, the mean isopycnal descent rate of 60 m decade^{-1} drives an oxygen decline of 3 ± 2 µmol kg^{-1} decade^{-1}. The oxygen declines associated with contraction of AABW are more than double the reduction caused by transport changes alone. Our calculated deoxygenation rates are consistent with previous work which observed in situ declines of 1 µmol kg^{-1} decade^{-1} averaged between 1,200 m depth and the seafloor[17] and 2–5 µmol kg^{-1} decade^{-1} for water denser than 28.30 kg m^{-3} (ref. 8). We conclude that reduction in the export of bottom waters can explain the full magnitude of deep oxygen losses. Furthermore, this analysis shows that contraction of AABW (and replacement with lower-oxygen CDW) makes a larger contribution to deoxygenation than reductions in the amount of oxygen transported to the abyss.

Discussion

We have synthesized direct observations of temperature, salinity, oxygen and velocity, with a modelled estimate of bottom water flow structure, to quantify changes in abyssal overturning and ventilation in the Australian Antarctic Basin. Between 1994 and 2009, dense water export of both ALBW and RSBW reduced by at least 50%, causing the lower limb of the overturning circulation to slow by −2.8 ± 0.5 Sv decade^{-1} (Fig. 4c). Weaker overturning reduced oxygen transport to the abyss and caused thinning of well-ventilated layers, reducing the oxygen content of the deep basin (Fig. 5). Between 2009 and 2017, ALBW export continued to weaken, while RSBW export increased. The recovery of RSBW partially offset the earlier slowdown, such that, over the full period (1994–2017), the deep overturning slowed at a rate of −0.8 ± 0.5 Sv decade^{-1} (Fig. 4c).
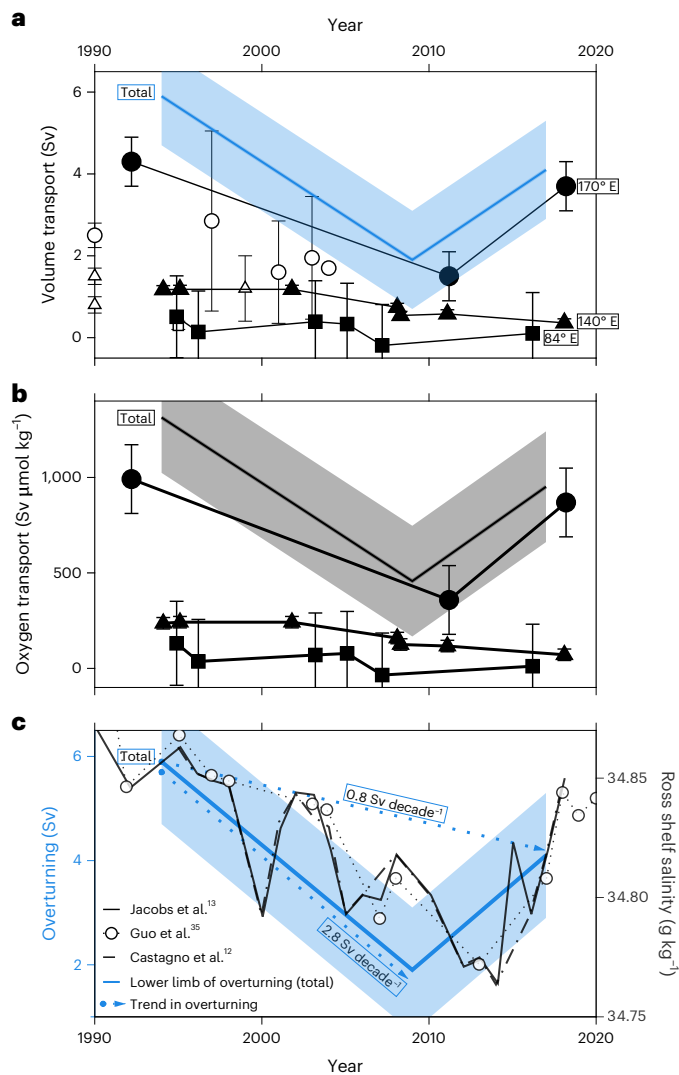
Fig. 4 | Decadal variability of bottom water volume and oxygen transport between 1990 and 2020. a, Volume transport. Black symbols show estimates ± calculated total uncertainty made using joint mooring–model–hydrographic method (square/triangle/circle symbols, 84° E/140° E/170° E; equation (2), Extended Data Fig. 7 and Supplementary Section 2). White symbols show comparative estimates from other studies[11,24,47–50] (Supplementary Table 3). Blue line, total volume transport for time periods of 1994–1996, 2007–2011 and 2016–2018, which estimates the strength of the lower limb of overturning circulation in the Australian Antarctic Basin (shading shows total error of 1.2 Sv; Supplementary Table 2). **b**, Oxygen transport. Black line, total oxygen transport that estimates abyssal ventilation ± total uncertainty of 290 Sv μmol kg⁻¹ (equation (3)). **c**, Comparison of lower limb of overturning circulation and shelf salinities from a site of DSW formation in Ross Sea (Terra Nova Bay; refs. 12,13,35). Dotted blue arrows show declining trend in overturning for 1994–2009 and 1994–2017 that have uncertainties of ±0.5 Sv decade⁻¹.

RSBW at 170° E, where the greatest variations in bottom water salinity, thickness, speed and transport are observed (Figs. 1–3). In addition, the volume transport of RSBW covaries with the salinity of DSW on the Ross Sea continental shelf (Fig. 4c). As AABW is a mixture of DSW and circumpolar deep water (CDW), changes in the properties or amount of CDW in the mixture could also influence the salinity of AABW. However, no significant trend in the salinity of CDW has been observed offshore of the Ross Sea[6]. We conclude that changes in RSBW transport, and thus the lower limb of the overturning circulation in the Australian Antarctic Basin, are driven by Ross Sea shelf water salinity.

Salinity changes on the Ross Sea continental shelf are largely driven by two processes: glacial meltwater input, primarily from the Amundsen Sea[13] and variations in sea-ice formation[33]. Multidecadal and significant freshening of RSBW observed before the 2010s has been attributed to increased glacial meltwater input and freshening of DSW, beginning as early as the 1950s[12–14,21]. The rapid increase in DSW and AABW salinity after 2014 (ref. 12) has been attributed to an increase in sea-ice formation driven by anomalous winds associated with an unusual juxtaposition of interannual climate anomalies (a strong El Niño and positive Southern Annular Mode during 2015–2018)[33]. Salinity of DSW in Terra Nova Bay peaked in 2018, when the climate anomaly terminated[35]. As the climate anomaly was transient, whereas glacial meltwater input from the Amundsen Sea is expected to persist and increase[36,37], we anticipate that freshening of shelf waters and slowing of the overturning will resume in the future, consistent with the overall freshening trend over the past 63 years[13].

We have documented a weakening of deep overturning and ventilation in the Australian Antarctic Basin, whose abyssal layers are supplied by ALBW and RSBW. These regions supply the abyssal waters of the entire Pacific and the eastern Indian basins[11], so the changes quantified here are likely to impact a large fraction of the global abyssal ocean. The largest freshening-driven changes in AABW formation and export are expected in the Ross Sea, as it lies downstream of the large and growing input of glacial meltwater into the Amundsen Sea[10,21,36,37]. However, multidecadal freshening and contraction of AABW has also been observed in the Atlantic[3,4], where sea-ice variability[38] has driven changes in salinity in the Weddell Sea. Indeed, contraction of the dense AABW layer is observable in each basin (Extended Data Fig. 7), consistent with global deep deoxygenation[17], suggesting weakening of the deep overturning and ventilation is underway in other Antarctic basins.

Our work highlights the present sensitivity of deep overturning and ventilation to changes in shelf water salinity in regions of AABW formation. Evidence from sediment cores suggests that this physical mechanism has operated on glacial–interglacial timescales, with freshening of near-surface waters causing reduced AABW formation and deep deoxygenation in past warm periods in Earth's climate[39]. Model studies also provide evidence that the amplitude of future freshening will set the rate of slowdown of the deep overturning circulation. For example, models that include projected increases in freshwater input from glacial melt[18,40] show a fourfold larger slowdown of the deep overturning compared to the multimodel mean of standard CMIP5 models[41] that do not include resolved ice-sheet melt.

Our results demonstrate that freshening of shelf waters, attributed to increased glacial melt in previous studies[13,14,21], has slowed the lower limb of the deep overturning circulation and driven deoxygenation of the abyssal Australian Antarctic Basin (Fig. 5). Freshening, contraction and deoxygenation of AABW observed in other Antarctic basins[3,4,6,38] suggests that freshening of shelf waters (by glacial melt[13,21] or sea-ice changes[33,38,42]) is driving a circumpolar slowdown of abyssal overturning and ventilation. Freshening of DSW is expected to continue and even accelerate over the coming decades, as the Antarctic Ice Sheet loses mass in a warming climate[10,20,36,37]. We may therefore

The changes in RSBW transport are driven by changes in salinity (hence density) of DSW on the Ross Sea continental shelf (Fig. 4c). Changes in shelf water salinity influence bottom water transport in two ways. First, the speed of bottom water export is reduced as the shelf water density decreases, as current speed is proportional to density in the gravity-driven plumes close to the sources of bottom water (Fig. 3c,e; refs. 29,30). Second, the area of the AABW layer is reduced as shelf water density decreases because the densest layers are no longer renewed and therefore thin (Extended Data Figs. 1–4; ref. 7). These mechanisms are most apparent for
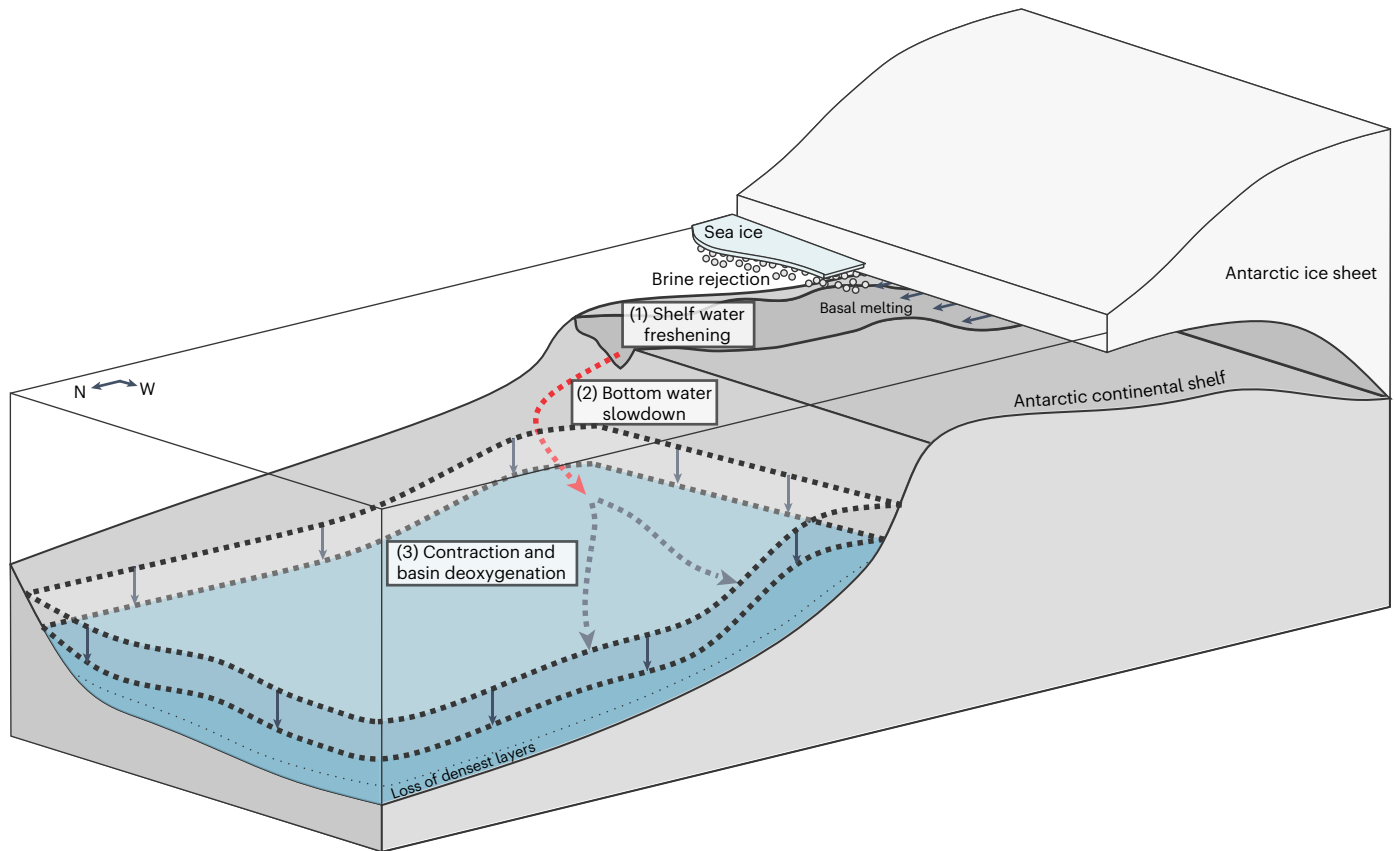
Fig. 5 | Schematic summarizing causes and consequences of AABW variability in the Australian Antarctic Basin. Freshening of shelf waters, attributed to increased glacial melt in previous studies[13,14,21], reduces export of dense water. Reduced export of DSWs slows the lower limb of the overturning circulation. Weaker overturning reduces oxygen transport to the abyss and thins deep well-ventilated layers, causing deep deoxygenation across the basin.

anticipate further decline in the deep overturning circulation around the Antarctic margin and further reductions in the oxygen content of abyssal waters, with the rate of change modulated by shorter term variability as seen in the late 2010s in the Ross Sea.

Online content

Any methods, additional references, Nature Portfolio reporting summaries, source data, extended data, supplementary information, acknowledgements, peer review information; details of author contributions and competing interests; and statements of data and code availability are available at https://doi.org/10.1038/s41558-023-01667-8.

References

1. Orsi, A. H., Johnson, G. C. & Bullister, J. L. Circulation, mixing, and production of Antarctic bottom water. *Progr. Oceanogr.* **43**, 55–109 (1999).
2. Johnson, G. C. Quantifying Antarctic bottom water and North Atlantic deep water volumes. *J. Geophys. Res.* https://doi.org/10.1029/2007JC004477 (2008).
3. Purkey, S. G. & Johnson, G. C. Global contraction of Antarctic bottom water between the 1980s and 2000s. *J. Clim.* **25**, 5830–5844 (2012).
4. Purkey, S. G. & Johnson, G. C. Antarctic bottom water warming and freshening: contributions to sea level rise, ocean freshwater budgets, and global heat gain. *J. Clim.* **26**, 6105–6122 (2013).
5. Azaneu, M., Kerr, R., Mata, M. M. & Garcia, C. A. E. Trends in the deep Southern Ocean (1958–2010): implications for Antarctic bottom water properties and volume export. *J. Geophys. Res. Oceans* **118**, 4213–4227 (2013).
6. Schmidtko, S., Heywood, K. J., Thompson, A. F. & Aoki, S. Multidecadal warming of Antarctic waters. *Science* **346**, 1227–1231 (2014).
7. van Wijk, E. M. & Rintoul, S. R. Freshening drives contraction of Antarctic bottom water in the Australian Antarctic Basin. *Geophys. Res. Lett.* **41**, 1657–1664 (2014).
8. Katsumata, K., Nakano, H. & Kumamoto, Y. Dissolved oxygen change and freshening of Antarctic bottom water along 62S in the Australian Antarctic Basin between 1995/1996 and 2012/2013. *Deep Sea Res. II* **114**, 27–38 (2015).
9. Bindoff, N. L. et al. in *IPCC Special Report on the Ocean and Cryosphere in a Changing Climate* (eds Portner, H.-O. et al.) Ch. 5 (IPCC, 2019).
10. Meredith, M. et al. in *IPCC Special Report on the Ocean and Cryosphere in a Changing Climate* (eds Portner, H.-O. et al.) Ch. 3 (IPCC, 2019).
11. Solodoch, A. et al. How does Antarctic bottom water cross the southern ocean? *Geophys. Res. Lett.* https://doi.org/10.1029/2021GL097211 (2022).
12. Castagno, P. et al. Rebound of shelf water salinity in the Ross Sea. *Nat. Commun.* **10**, 5441 (2019).
13. Jacobs, S. S., Giulivi, C. F. & Dutrieux, P. Persistent Ross Sea freshening from imbalance West Antarctic ice shelf melting. *J. Geophys. Res. Oceans* **127**, e2021JC017808 (2022).
14. Jacobs, S. S., Giulivi, C. F. & Mele, P. A. Freshening of the Ross Sea during the late 20th century. *Science* **297**, 386–389 (2002).
15. Matear, R. J., Hirst, A. C. & McNeil, B. I. Changes in dissolved oxygen in the Southern Ocean with climate change. *Geochem. Geophy. Geosyst.* https://doi.org/10.1029/2000GC000086 (2000).

16. Oschlies, A., Brandt, P., Stramma, L. & Schmidtko, S. Drivers and mechanisms of ocean deoxygenation. *Nat. Geosci.* **11**, 467–473 (2018).

17. Schmidtko, S., Stramma, L. & Visbeck, M. Decline in global oceanic oxygen content during the past five decades. *Nature* **542**, 335–339 (2017).

18. Lago, V. & England, M. H. Projected slowdown of Antarctic bottom water formation in response to amplified meltwater contributions. *J. Clim.* **32**, 6319–6335 (2019).

19. Shimada, K. et al. Shoaling of abyssal ventilation in the Eastern Indian sector of the Southern Ocean. *Commun. Earth Environ.* **3**, 120 (2022).

20. Rignot, E. et al. Four decades of Antarctic ice sheet mass balance from 1979–2017. *Proc. Natl Acad. Sci. USA* **116**, 1095–1103 (2019).

21. Pan, X. L., Li, B. F. & Watanabe, Y. W. Intense ocean freshening from melting glacier around the Antarctica during early twenty-first century. *Sci. Rep.* **12**, 383 (2022).

22. Kiss, A. E. et al. Access-om2 v1.0: a global ocean–sea ice model at three resolutions. *Geosci. Model Dev.* **13**, 401–442 (2020).

23. Morrison, A. K., Hogg, A. M., England, M. H. & Spence, P. Warm circumpolar deep water transport toward Antarctica driven by local dense water export in canyons. *Sci. Adv.* **6**, eaav2516 (2020).

24. Gordon, A. L. et al. Western Ross Sea continental slope gravity currents. *Deep Sea Res. Part II* **56**, 796–817 (2009).

25. Gordon, A. L., Huber, B. A. & Busecke, J. Bottom water export from the western Ross Sea, 2007 through 2010. *Geophys. Res. Lett.* **42**, 5387–5394 (2015).

26. Bowen, M. M. et al. The role of tides in bottom water export from the western Ross Sea. *Sci. Rep.* **11**, 2246 (2021).

27. Bowen, M. M. et al. Tides regulate the flow and density of Antarctic bottom water from the western Ross Sea. *Sci. Rep.* **13**, 3873 (2023).

28. Heywood, K. J., Sparrow, M. D., Brown, J. & Dickson, R. R. Frontal structure and Antarctic bottom water flow through the Princess Elizabeth Trough, Antarctica. *Deep Sea Res. Part I* **46**, 1181–1200 (1999).

29. Ellison, T. H. & Turner, J. S. Turbulent entrainment in stratified flows. *J. Fluid Mech.* **6**, 423–448 (1959).

30. Smith, P. C. Streamtube model for bottom boundary currents in ocean. *Deep Sea Res. Part I* **37**, 431–446 (1975).

31. Price, J. F. & Baringer, M. O. Outflows and deep water production by marginal seas. *Progr. Oceanogr.* **33**, 161–200 (1994).

32. Sherwin, T. J. Observations of the velocity profile of a fast and deep oceanic density current constrained in a gully. *J. Geophys. Res.* https://doi.org/10.1029/2009JC005557 (2010).

33. Silvano, A. et al. Recent recovery of Antarctic bottom water formation in the Ross Sea driven by climate anomalies. *Nat. Geosci.* **13**, 780–786 (2020).

34. Foppert, A. et al. Deep Argo reveals bottom water properties and pathways in the Australian-Antarctic Basin. *J. Geophys. Res. Oceans* **126**, e2021JC017935 (2021).

35. Guo, G., Gao, L. & Shi, J. Modulation of dense shelf water salinity variability in the western Ross Sea associated with the Amundsen sea low. *Environ. Res. Lett.* **16**, 014004 (2021).

36. Golledge, N. R. et al. Global environmental consequences of twenty-first-century ice-sheet melt. *Nature* **566**, 65–72 (2019).

37. Holland, P. R., Bracegirdle, T. J., Dutrieux, P., Jenkins, A. & Steig, E. J. West Antarctic ice loss influenced by internal climate variability and anthropogenic forcing. *Nat. Geosci.* **12**, 718–724 (2019).

38. Abrahamsen, E. P. et al. Stabilization of dense Antarctic water supply to the Atlantic Ocean overturning circulation. *Nat. Clim. Change* **9**, 742–746 (2019).

39. Glasscock, S. K., Hayes, C. T., Redmond, N. & Rohde, E. Changes in Antarctic bottom water formation during interglacial periods. *Paleoceanogr. Paleoclimatol.* **35**, e2020PA003867 (2020).

40. Li, Q., England, M. H., Hogg, A. M., Rintoul, S. R. & Morrison, A. K. Abyssal ocean overturning slowdown and warming driven by Antarctic meltwater. *Nature* **615**, 841–847 (2023).

41. Heuzé, C., Heywood, K. J., Stevens, D. P. & Ridley, J. K. Changes in global ocean bottom properties and volume transports in CMIP5 models under climate change scenarios. *J. Clim.* **28**, 2917–2944 (2015).

42. Haumann, F., Gruber, N. & Münnich, M. E. A. Sea-ice transport driving Southern Ocean salinity and its recent trends. *Nature* **537**, 89–92 (2016).

43. Jones, S. R. *MAFF Current Meter Data Inventory, 1990–1993: CEFAS Data Holding ID Number 243* (MAFF, 1996).

44. Fukamachi, Y. et al. Seasonal variability of bottom water properties off Adlie Land, Antarctica. *Geophys. Res. Lett.* **105**, 6531–6540 (2000).

45. Gordon, A. L. et al. Energetic plumes over the western Ross Sea continental slope. *Geophys. Res. Lett.* https://doi.org/10.1029/2004GL020785 (2004).

46. Huber, B. & Gordon, A. *Processed Current Meter Data From the Adare Basin Near Antarctica Acquired During the Nathaniel B. Palmer Expedition NBP1101 (2011)* (EIDA, 2015).

47. Donohue, K. A., Hufford, G. E. & McCartney, M. S. Sources and transport of the deep western boundary current east of the Kerguelen Plateau. *Geophys. Res. Lett.* **26**, 851–854 (1999).

48. Marsland, S. J., Bindoff, N. L., Williams, G. D. & Budd, W. F. Modeling water mass formation in the Mertz Glacier Polynya and Adélie Depression, East Antarctica. *J. Geophys. Res. Oceans* https://doi.org/10.1029/2004JC002441 (2004).

49. Williams, G. D., Bindoff, N. L., Marsland, S. J. & Rintoul, S. R. Formation and export of dense shelf water from the Adélie Depression, East Antarctica. *J. Geophys. Res.* https://doi.org/10.1029/2007JC004346 (2008).

50. Rivaro, P., Massolo, S., Bergamasco, A., Castagno, P. & Budillon, G. Chemical evidence of the changes of the Antarctic bottom water ventilation in the western Ross Sea between 1997 and 2003. *Deep Sea Res. Part I* **57**, 639–652 (2010).

Methods

Definition of AABW sources

Three varieties of bottom water flow into the Australian Antarctic Basin via topographic gateways (Fig. 1a; refs. 1,11). The saltiest variety, RSBW, is exported from the western side of the Ross Sea, then flows around Cape Adare and into the basin, where it crosses the S04P section at 170° E. ALBW, which is colder and fresher, is exported at the Adélie Sill, joins RSBW and flows westward south of the Hakurei seamount where it is recorded at SR03 at 140° E.

At 140° E, ALBW and RSBW flow together into the Australian Antarctic Basin, so, to avoid double counting bottom water transport, we separate these water masses using their unique properties. ALBW is recently ventilated compared with the older bottom water along SR03 and is therefore colder and denser than RSBW and recirculated AABW. ALBW is defined by conservative temperature <−0.5 °C and absolute salinity <34.83 g kg^{-1} (refs. 34,51), which corresponds to neutral densities of >28.34 kg m^{-3}. Using this neutral density threshold, the ALBW core lies within the topographic saddle south of the Hakurei seamount, between 65° S and 63° S and adjacent to the seafloor (Fig. 2d,e,f and Extended Data Figs. 1–3). This definition of the ALBW core ensures that bottom water across SR03 has not been overestimated (Supplementary Table 2).

Exchange of bottom water between the Australian Antarctic Basin and the Weddell–Enderby Basin occurs at a gap in topography between the Kerguelen Plateau and Antarctic continent, known as the Princess Elizabeth Trough[28]. South of 64.5° S, a portion of RSBW and ALBW flows westward, leaving the basin. Meanwhile, relatively warm WSDW flows eastward into the basin in the northern portion of the trough (Fig. 1a,b). After entering the basin, WSDW, ALBW and RSBW combine to form AABW which flows northwards to eventually fill the abyssal portions of the Australian Antarctic Basin and beyond.

We rule out the Australian Antarctic discordance as a region of mean flow where dense, oxygen-rich AABW can exit the basin. The Australian Antarctic discordance is an anomalously deep zone of the Southeast Indian Ridge between 120° E and 130° E and separates the Indian Ocean from the Australian Antarctic Basin (Fig. 1a). A hydrographic section collected across the discordance in November–December 1994 does not record neutral densities of >28.3 kg m^{-3} and the oxygen concentration does not exceed 210 µmol kg^{-1} (Supplementary Fig. 1). There are no other publicly available hydrographic data at this location but analysis of the time mean neutral density field from the model confirms that there is no mean flow of AABW at this location. For this study, in which we consider mean flows only, we conclude that oxygen-rich AABW denser than 28.30 kg m^{-3} does not exit the basin at this location and we do not consider it further. Ultimately, AABW exits the basin via mixing and lightening, which we do not consider here.

Repeat hydrography

We use repeat hydrographic sections along the historical transects I08S, SR03 and S04P. At the topographic gateway of each section, we investigate property changes of bottom waters entering the Australian Antarctic Basin at nominal longitudes of 84° E, 140° E and 170° E, respectively (Fig. 1). Each section was repeated at least three times from the early 1990s to late 2010s (Supplementary Table 1). In situ temperature and practical salinity were converted into conservative temperature and absolute salinity using the Gibbs sea water (GSW) Oceanographic Toolbox of TEOS-10. We then calculate neutral density (γ) following ref. 52 and use a threshold of γ ≥ 28.30 kg m^3 to define AABW. Discrete measurements of pressure, temperature, salinity and dissolved oxygen concentration from bottle data files were interpolated to a regularly spaced two-dimensional grid of 10 dbar × 5.5 km at each location (Fig. 2 and Extended Data Figs. 1–3).

All measurements have been collected according to GO-SHIP standards which are accurate to 0.002 °C, 0.002 g kg^{-1}, ~2.6 µmol kg^{-1} and 3 dbar (ref. 53). When estimating change over time, the greater uncertainties arise from sampling biases and limited temporal sampling of each region (aliasing errors). To minimize seasonal aliasing, we exclusively use sections completed in austral summer and autumn (predominantly January, February or March; Supplementary Table 1), then we quantify the instrument, sampling and aliasing error for each property and calculate their total uncertainty. These values are 0.09 °C, 0.01 g kg^{-1} and 3 µmol kg^{-1} and allow us to assess the significance of observed decadal variability (Supplementary Section 2).

Volume transport of bottom waters

Bottom water volume transport provides critical information on the strength and variability of abyssal circulation, yet few transport-resolving current meter arrays have been deployed in the Southern Ocean. In the Australian Antarctic Basin, moored current meters have been sporadically deployed at each source water location from the early 1990s to 2010s and provide velocity time series of 1–3 years duration (Fig. 1a and Table 1). These time series show that the velocity of AABW entering the basin varies seasonally (Fig. 3a,c,e). Furthermore, at 140° E and 170° E, the speed has a clear relationship with the density at the deepest mooring since these flows behave as density-driven plumes (Fig. 3c,e). Therefore, these time series can be used to quantify characteristic velocities of bottom water flow for a given season and near-bottom neutral density. However, as only a single mooring is available at each gateway, transport cannot be estimated by direct integration of the velocity records. As described below, we estimate AABW transport at each gateway by combining mooring observations of flow speed, hydrographic measurements of density and horizontal structure functions derived from modelled velocity fields.

Volume transport is estimated at each section in three steps. First, moored current meters and conductivity, temperature and depth sensors provide time series of the cross-sectional speed, v, and neutral density of the bottom waters. The component of the current normal to the section is averaged over daily intervals to remove the effects of tides (Fig. 3a,c,e). Vertical velocity shear, dv/dz, is calculated between the two deepest current meters on each mooring (either 20–40 m or 400–800 m above the seafloor; Table 1). Laboratory tank experiments[29,30], numerical models[31] and observations[32] demonstrate that the speed of density-driven plumes is proportional to the density difference between the dense and ambient water and this behaviour is clearly observed at 140° E and 170° E. Cross-sectional speed and its shear also vary with season at each gateway. Given these dependencies, we bin cross-sectional speed and its shear by season and density (in 0.01 kg m^{-3} bins) to provide a look-up table for speed and shear as a function of season and near-bottom neutral density (Fig. 3a,c,e). An alternative approach, that uses regression to relate density and speed, yields the same results (Supplementary Table 2); however, we avoid this methodology as it enforces a particular functional relationship (for example, linear) between speed and density.

Second, we use modelled velocity fields to recover the horizontal flow structure of bottom water as structure functions ($\mathcal{F}$; Extended Data Fig. 6). The functions are extracted from the interannually forced ACCESS-OM2-01 JRA55-IAF model output, a global 0.1° ocean sea-ice model with 75 vertical levels. The ocean component of the model is the Modular Ocean Model (MOM) v.5.1 and the sea-ice component is the Los Alamos sea-ice model (CICE) v.5.1.2. The model has been forced by a prescribed interannually varying atmosphere from JRA55-do re-analysis v.1.4 for the period 1958 to 2018 (ref. 54). This model is used because it has been shown to simulate bottom water formation locations, magnitude and export reasonably well[23,55], comparing favourably to observations (Extended Data Fig. 5). For each month between 1990 and 2018, the modelled north and east velocity components are extracted along each hydrographic section and rotated to give two-dimensional fields of cross-sectional velocity (that is, v varies with latitude and depth). For each time step and at each latitude (about every 5.5 km), the mean cross-sectional speed, v, is calculated within

the AABW layer ($\gamma \geq 28.30$ kg m^{-3}). Horizontally varying speeds are then normalized using the maximum speed observed in the record, where positive values represent flow into the basin and vice versa and seasonal means are taken over 1990 to 2018. We note that the structure function is similar for $\gamma \geq 28.0$ kg m^{-3}, indicating that the shape of bottom flow is insensitive to the choice of density used to define AABW. Thus, the structure functions provide the normalized seasonally and horizontally varying structure of bottom water flow (Fig. 3b,d,f).

Third, hydrographic sections provide measurements of the near-bottom neutral density, which is used to select the relevant binned cross-sectional speed and shear corresponding to the observed density (description of look-up table above and Fig. 3a,c,e). Near-bottom neutral density is calculated over the deepest 50 m of AABW at each section and time (note that density is unaffected by ±20 m changes in this vertical extent; see Supplementary Section 2.6 for potential biases caused by this choice). Bottom speed, v_b and dv/dz are combined to estimate the mean speed of the bottom water layer, v, as

$$v = \frac{v_b - (h \times dv/dz)}{2}. \qquad (1)$$

Here, h is the vertical thickness of AABW above the isobath of the mooring, giving v at a point along the AABW layer. Then, by multiplying v by the structure function, the function is scaled to the absolute speed of the bottom water flow. This multiplication gives the speed of AABW as it varies with latitude ($v_{AABW} = v\mathcal{F}$; Extended Data Fig. 6).

Finally, volume transport is estimated at each gateway for each occupation of the repeat hydrographic sections, t, using:

$$T_V(t) = \int v_{AABW}(t)\, dA. \qquad (2)$$

The units of T_V are Sv (1 Sv is 10^6 m^3 s^{-1}). The spacing in time t is set by the occupation of each repeat hydrographic section, which is approximately decadal. So, we quantify the uncertainty due to aliasing of shorter term seasonal cycles and interannual variability, as well as sampling and instrument errors and calculate a total error of 0.5 Sv decade^{-1} for decadal volume transport trends (Supplementary Section 2).

This methodology assumes that the relationship between cross-sectional speed and density derived from the mooring applies to the AABW layer as a whole. We make this assumption on the basis of three factors. First, the best information about AABW speed and its relationship to density is from mooring data (continuous, direct observations that resolve seasonal and higher frequency variability; Fig 3). Second, the best information about the density distribution of the AABW layer is from the repeat hydrographic sections (latitude–depth cross-sections that span the whole layer; Extended Data Fig. 3). Third, γ_{bot} measured at the mooring and by the repeat hydrographic data are observed to vary in the same way (Supplementary Fig. 3). These factors suggest that the approach we adopt provides the most robust estimate of AABW transport, given the information available. The sensitivity to these assumptions is assessed in Supplementary Section 2.

Thinning rates driven by decreasing transport

Given the changes in overturning strength and an estimate of the area of the basin filled with AABW, we can estimate the rate of thinning of this water mass. The area is defined as the region of the Australian Antarctic Basin enclosed by the 3,500 m isobath (Fig. 1a), since 3,500 m is the approximate mean shallowest depth of AABW[8]. The contraction of isopycnals is then calculated by multiplying the strength of the lower limb of Southern Ocean overturning by the time period and dividing by the area. These estimates represent a basin mean thinning rate (m decade^{-1}) resulting solely from variability in bottom water transport and have an uncertainty of ±35 m decade^{-1} (Supplementary Section 2).

Oxygen transport estimates ventilation

We use oxygen transport, T_O, as a direct measure of abyssal ocean ventilation (renewal of water masses). Parameter T_O can be used as a proxy for ventilation of the Australian Antarctic Basin because abyssal oxygen is replenished solely by inflow of oxygen-rich bottom water (primarily ALBW and RSBW). T_O is the integral of cross-sectional speed and oxygen concentration, given by:

$$T_O(t) = \int v_{AABW}(t)\, O(t)\, dA, \qquad (3)$$

where O is the dissolved oxygen concentration of the AABW layer at each latitude across the section. The units are Sv µmol kg^{-1} (that is, 10^6 m^3 s^{-1}µmol kg^{-1}). We do not consider changes in oxygen solubility here since changes in circulation have been shown to be the dominant driver of reduced deep ventilation[16] and comparison of oxygen solubility in density bins along S04P shows changes smaller than the measurement uncertainty.

Deoxygenation driven by decreasing transport

Given the volume of the basin filled with AABW, we can estimate the rate of deoxygenation within the Australian Antarctic Basin. We define the basin volume as the region of the Australian Antarctic Basin beneath 3,500 m depth and enclosed by the 3,500 m isobath, based on the mean depth of the 28.30 kg m^{-3} surface[8], which amounts to 6.70×10^{15} m^3. Deoxygenation associated with the changes in ventilation strength is calculated by dividing the decadal changes in oxygen transport by the volume of the basin. The contraction of AABW also drives deoxygenation; as the AABW layer thins, well-ventilated AABW is replaced by CDW that is lower in oxygen, resulting in a reduction in oxygen on pressure surfaces. The oxygen change resulting from this isopycnal descent can be estimated by multiplying the vertical oxygen gradient by the isopycnal descent rate. The mean vertical oxygen gradient for CDW in the centre of the basin is taken from neutral densities of 27.00–28.30 kg m^{-3} along I09S and is 0.05 µmol kg^{-1} m^{-1}. The uncertainty on these decadal deoxygenation estimates is 2 µmol kg^{-1} decade^{-1} (Supplementary Section 2).

Data availability
All repeat hydrographic data are publicly available from the CLIVAR and Carbon Hydrographic Data Office at https://cchdo.ucsd.edu/ using Expocodes listed in Supplementary Table 1. The ACCESS-OM2 suite of models are available at https://github.com/COSIMA/access-om2. Mooring data are available on request from principal investigators (ADOX[28,43], ALCS[44], CALM[45,46]).

Code availability
Code available on request from K.L.G.

References

51. Snow, K., Rintoul, S. R., Sloyan, B. M. & Hogg, A. M. C. Change in dense shelf water and Adélie Land bottom water precipitated by iceberg calving. *Geophys. Res. Lett.* **45**, 2380–2387 (2018).

52. Jackett, D. R. & McDougall, T. J. A neutral density variable for the world's oceans. *J. Phys. Oceanogr.* **27**, 237–263 (1997).

53. Hood, E. M., Sabine, C. L. & Sloyan, B. M. *The GO-SHIP Repeat Hydrography Manual: A Collection of Expert Reports and Guidelines* (GO-SHIP, 2010).

54. Tsujino, H. et al. Jra-55 based surface dataset for driving ocean-sea-ice models (jra55-do). *Ocean Model.* **130**, 79–139 (2018).

55. Stewart, K. D. et al. Vertical resolution of baroclinic modes in global ocean models. *Ocean Model.* **113**, 50–65 (2017).

Acknowledgements

Competing interests

The authors declare no competing interests.

Additional information

Extended data is available for this paper at https://doi.org/10.1038/s41558-023-01667-8.

Supplementary information The online version contains supplementary material available at https://doi.org/10.1038/s41558-023-01667-8.

Correspondence and requests for materials should be addressed to Kathryn L. Gunn.

Peer review information *Nature Climate Change* thanks Einar Povl Abrahamsen, Rodrigo Kerr and Casimir de Lavergne for their contribution to the peer review of this work.
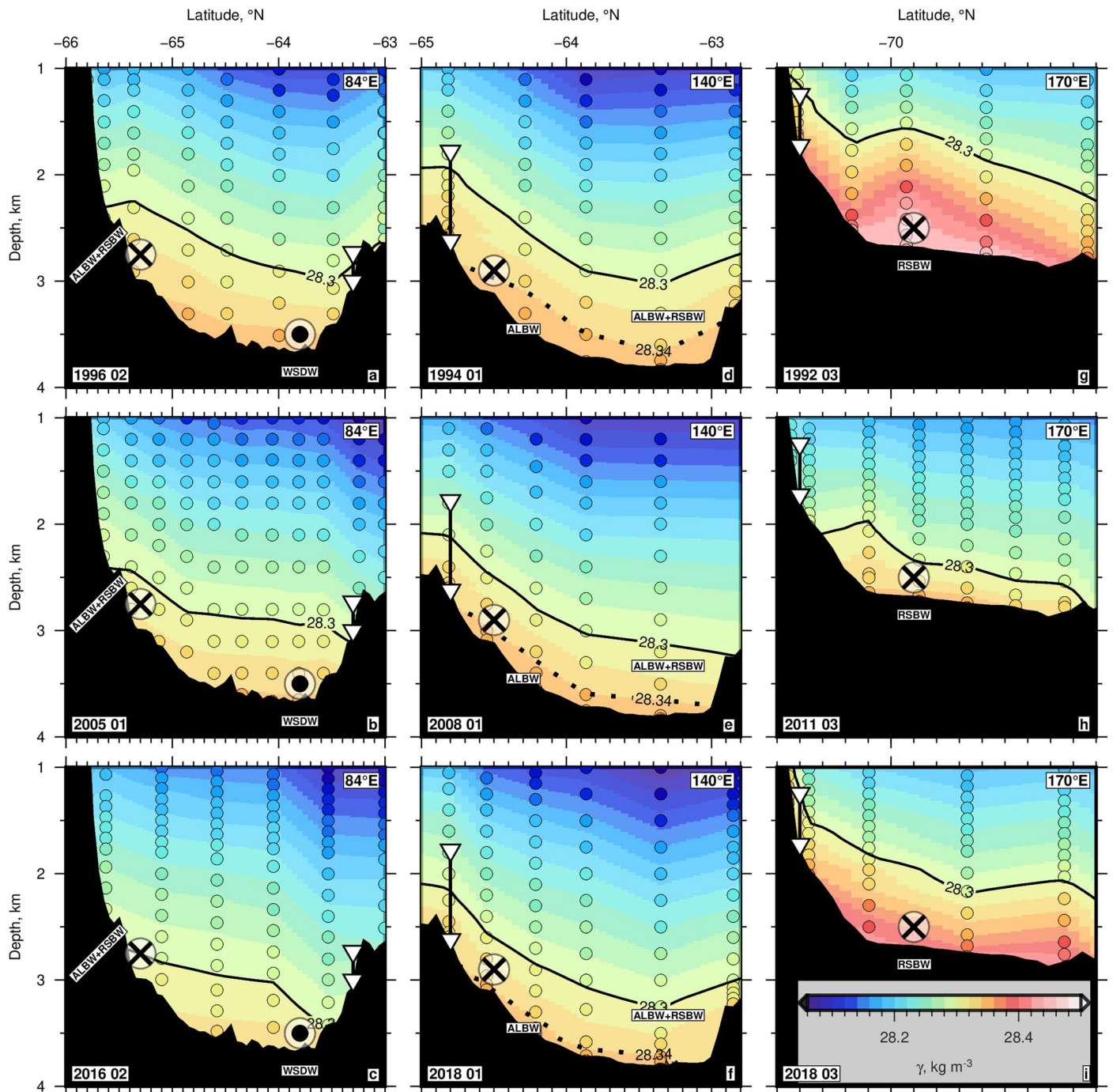
**Reprints and permissions information** is available at www.nature.com/reprints.
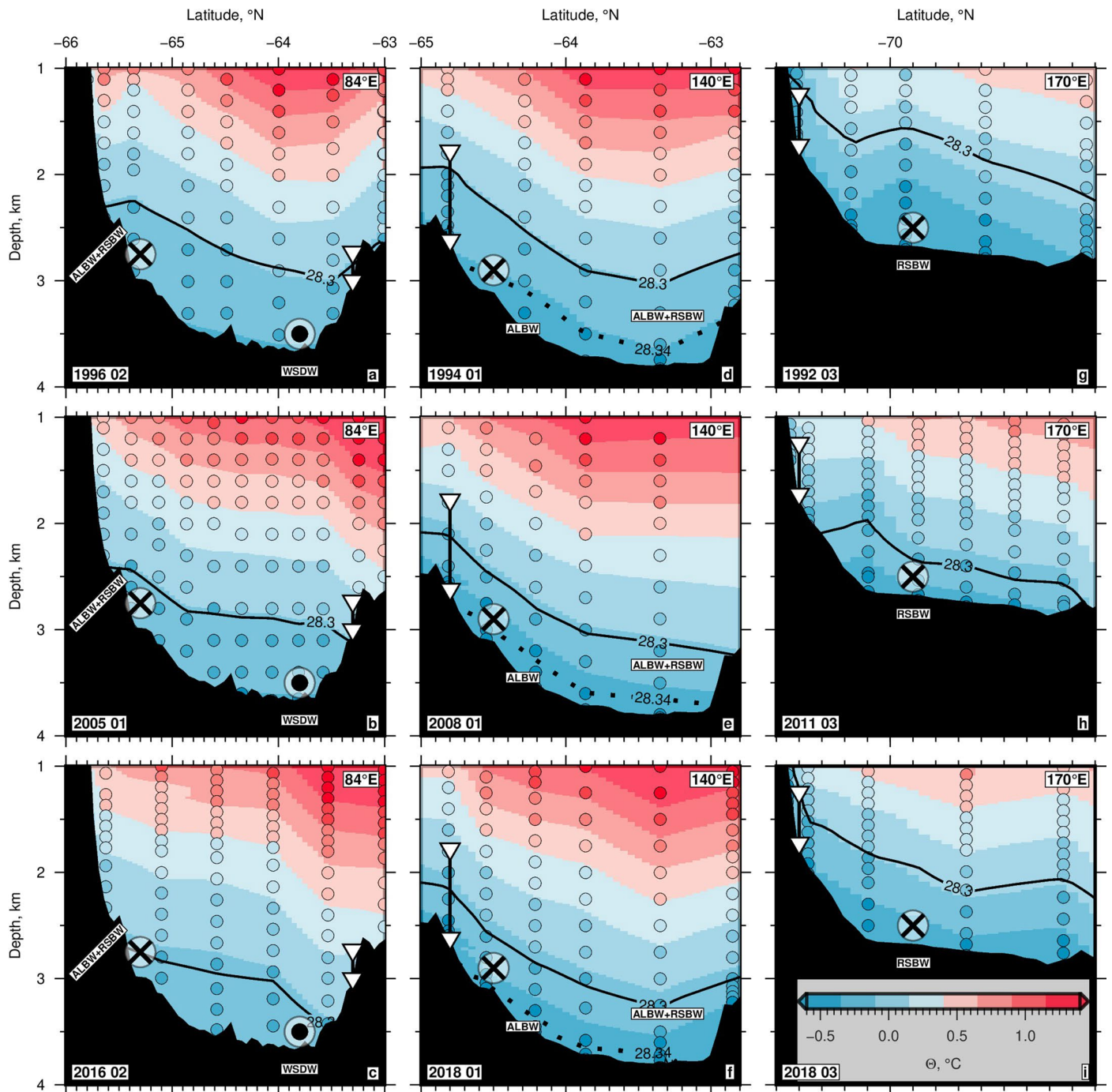
Extended Data Fig. 1 | Distribution of conservative temperature (Θ) at each repeat hydrographic section. Format same as Fig. 2.
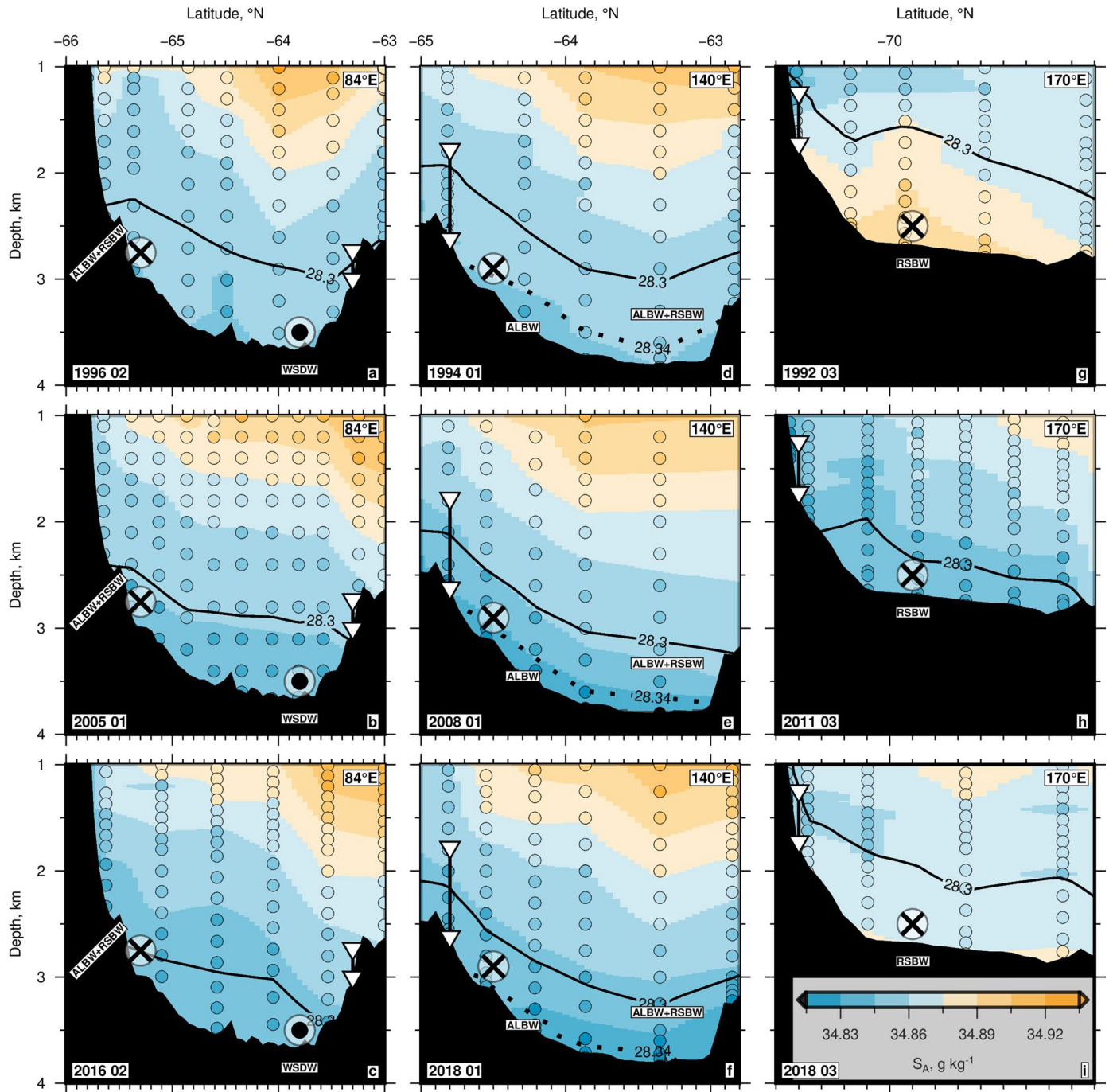
Extended Data Fig. 2 | Distribution of absolute salinity (S$_A$) at each repeat hydrographic section. Format same as Fig. 2.

Extended Data Fig. 3 | Distribution of neutral density (γ) at each repeat hydrographic section. The 28.30 kg m⁻³ surface marks the top of the AABW layer. Format same as Fig. 2.
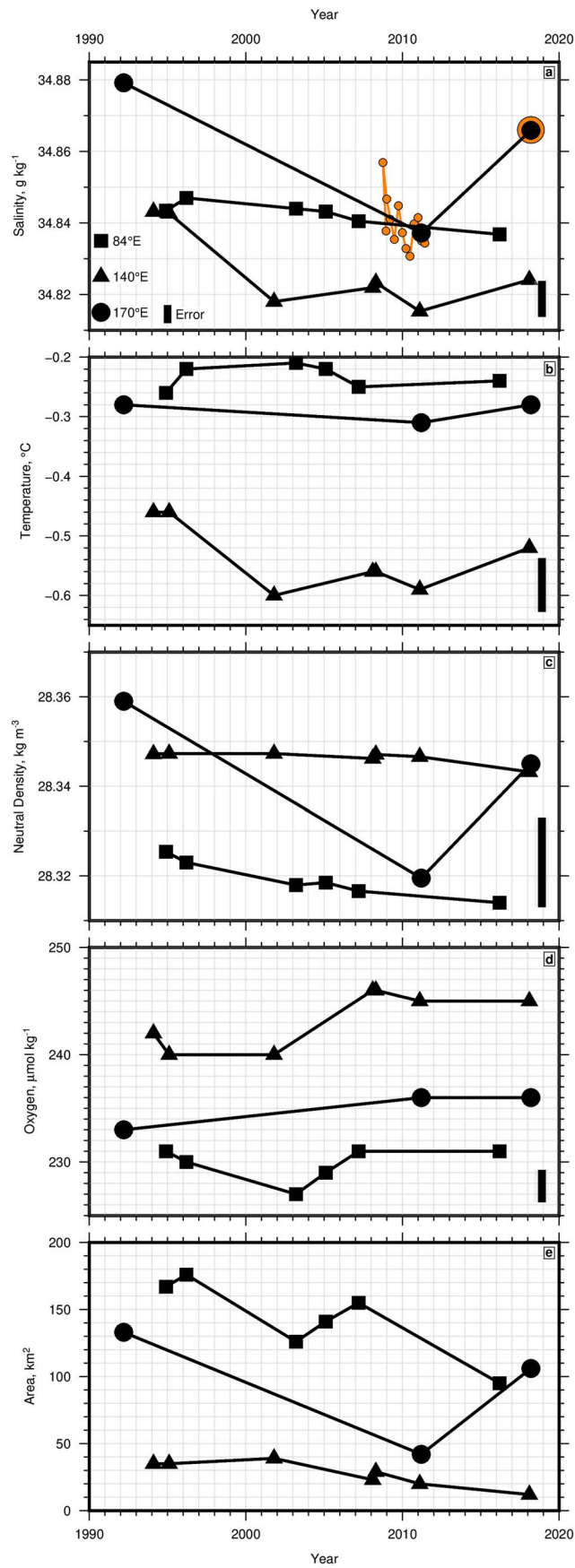
**Extended Data Fig. 4 | See next page for caption.**

Extended Data Fig. 4 | Physical and chemical property variability of bottom waters supplying the Australian Antarctic Basin. Time series shown for neutral density mean properties, where means are taken over the layer denser than 28.30 kg m^{-3}. (a) Absolute Salinity. Orange line and points = monthly mean absolute salinity time series from 2008-2011 CALM[24,46] and 2018 Ross Sea Outflow[26] experiment showing freshening and salinification of bottom (20 m above the seafloor) waters that is consistent with changes recorded by repeat hydrographic data. (b) Conservative Temperature, (c) Neutral Density, (d) Dissolved Oxygen Concentration, and (e) Area of AABW layer. Black symbols show mean bottom water properties at each gateway according to key in panel (a) where values at 140°E are for the narrow definition of this bottom water (that is neutral density ≥ 28.34 kg m^{-3}). Total uncertainty shown for each property includes an estimate of seasonal aliasing (note error of area is negligible at 1 km^2).
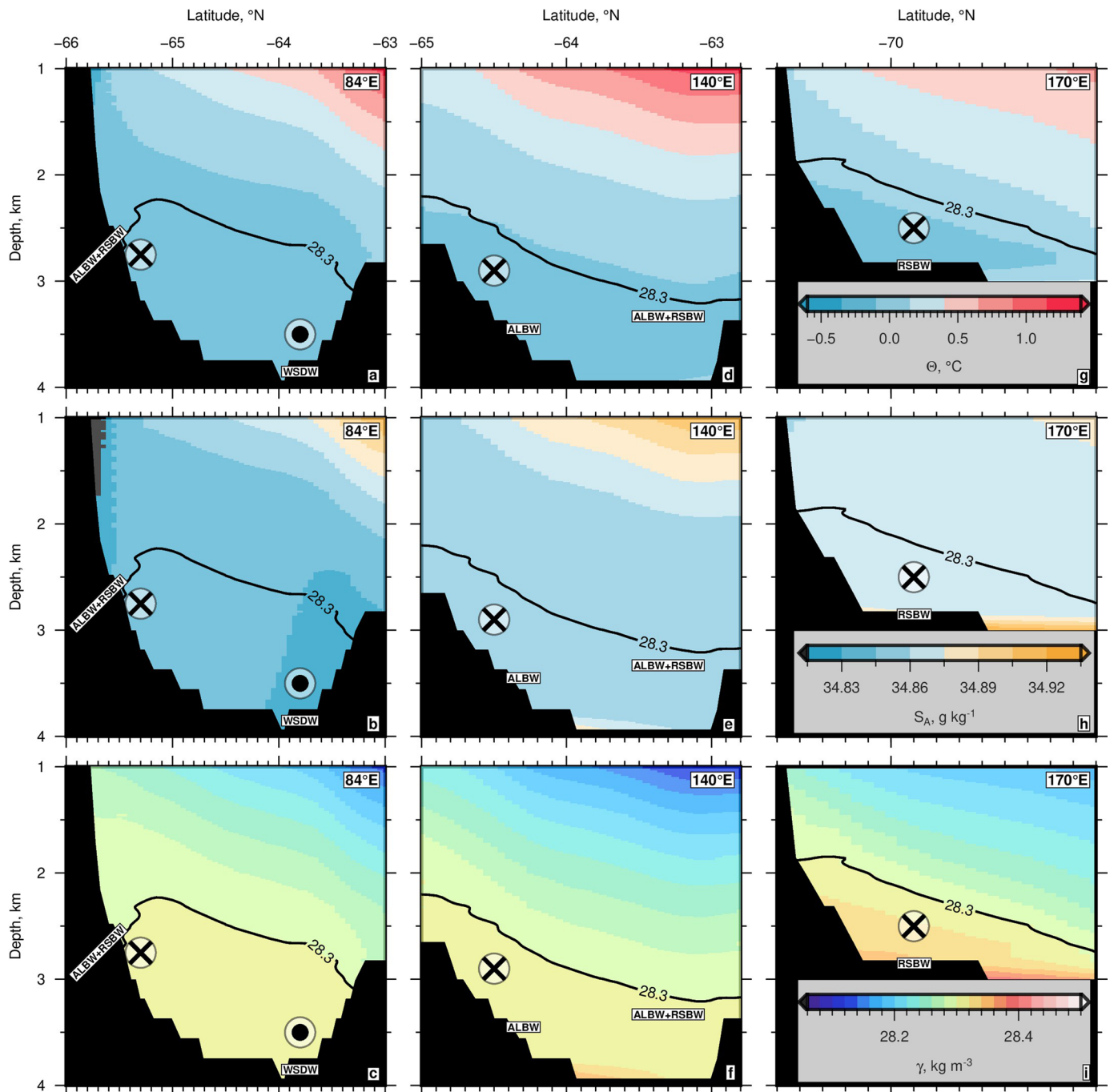
Extended Data Fig. 5 | Latitude–depth sections of time mean (1990–2018) hydrographic properties at each hydrographic section, as simulated by the model. The plot is organized in the same way as the observations in Figs. S3–5: left column is the 84°E section; middle column is 140°E; right column is 170°E. Black polygon = bathymetry across section; thin and thick black lines = neutral density contour of 28.30 kg m⁻³. (a, d, g) Conservative temperature (Θ); colour bar in panel (g). (b) Absolute salinity (S_A); colour bar in panel (h). (c) Neutral density (γ); colour bar in panel (i). Bottom water varieties and flow direction shown schematically on panels (a)-(i). Note different latitude scales.
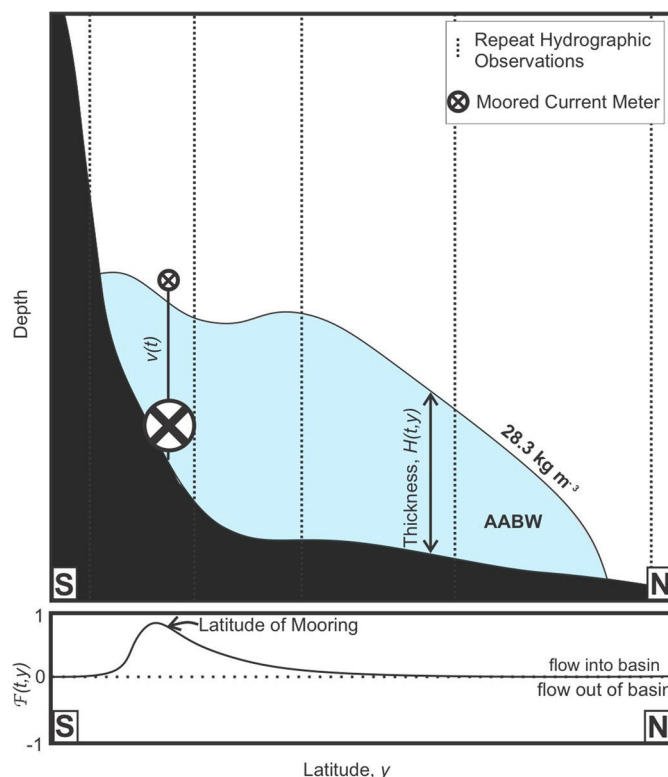
Extended Data Fig. 6 | Diagram showing approach that combines mooring, model, and hydrographic data to calculate volume transport of AABW. At each gateway section, the plume of AABW (blue shading) is measured by at least three repeat hydrographic stations (dashed lines) and one deep mooring (arrow symbols). The hydrographic profiles give temperature, salinity, neutral density, and oxygen as functions of latitude and pressure. The neutral density surface 28.30 kg m^{-3} is used to define the top of the AABW layer and is used to estimate the vertical thickness of the water mass at each latitude, $H(t,y)$. Deep-moored current meters spanning at least one year provide time series of the cross-sectional speed of the plume at a single latitude. Neighbouring current meters provide an estimate of the vertical shear at the same latitude. The horizontal structure of the flow (bottom panel, $\mathcal{F}$) is extracted from the global model at the location of the hydrographic section. $\mathcal{F}$ is the normalized, mean velocity within the layer denser than 28.30 kg m^{-3}. This structure function varies with season and latitude. Multiplying the layer-mean speed of the AABW at the mooring location by the normalized structure function gives the speed of the AABW layer as a function of latitude ($v\mathcal{F} = v_{AABW}$). This product is multiplied by H and integrated by latitude to calculate volume transport (T_v), as $T_V = \int [v(t)\mathcal{F}(t,y)] \times H(t,y)dy$. The calculation is repeated for each available hydrographic section, where t is the occupation, to yield a time series of T_v.
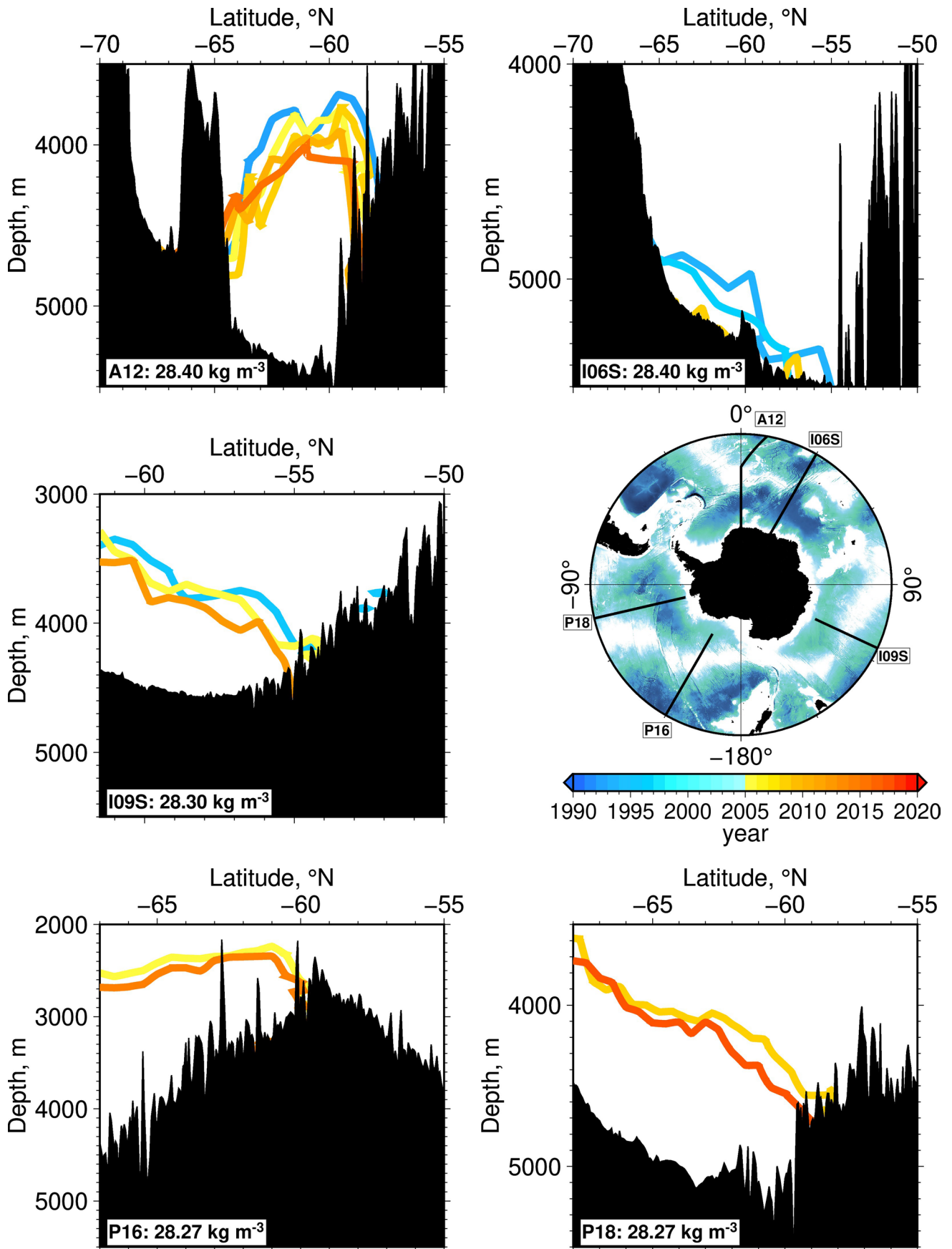
Extended Data Fig. 7 | See next page for caption.

Extended Data Fig. 7 | Latitude–depth sections across each Southern Ocean basin showing contraction of densest waters. Thick lines map contraction of densest water masses where blue-yellow-red colours track depths of each isoline during select years from 1990 to 2020 (isoline density indicated in each panel and colour scale in middle row). Moving eastwards, top row shows A12 and I06S across the Weddell–Enderby Basin, middle row shows I09S across the Australian Antarctic Basin, and bottom row shows P16 and P18 across the Amundsen-Bellingshausen Basin. Central map shows circum-Antarctic coverage of the repeat hydrographic sections.